Planar triangular model with long-range interactions

E. Rastelli,* S. Regina, and A. Tassi
Dipartimento di Fisica dell'Università and Istituto Nazionale per la Fisica della Materia, Parco Area delle Scienze 7/A, 43100 Parma, Italy

(Received 16 May 2002; published 20 August 2002)

The effect of dipole and long-range antiferromagnetic isotropic interactions in a triangular planar rotator model is investigated. The ground state is a ferromagnetic (F) configuration for pure dipole interaction and a 120° three-sublattice (T) configuration for pure antiferromagnetic interaction decaying as $1/r^3$ where r is the spin-spin distance. In between the spins are placed in striped configurations where n rows of spins parallel alternate with n rows of spins antiparallel to a nearest neighbors (NN) direction for any integer n provided that L/n is an even number, L being the lattice size. Monte Carlo simulation confirms the low temperature configurations found by analytic calculation. Specific heat, staggered susceptibility and order parameter are investigated to get the phase diagram and the order of the transition to the paramagnetic phase. The order-disorder phase transition is continuous only for the F phase (pure dipole interaction). It is first order for any nonzero long-range antiferromagnetic exchange interaction.

DOI: 10.1103/PhysRevB.66.054431 PACS number(s): 75.10.Hk, 75.30.Ds

I. INTRODUCTION

The planar triangular model in which the magnetic moments located on a triangular lattice are coupled by pure dipole interactions is characterized by a ferromagnetic (F) phase with long range order (LRO) at low temperature.[1] On the contrary, the minimum energy spin configuration for a square lattice[2] consists of alternating rows of spins up and down along a nearest neighbor (NN) direction. The close-packed structure of the triangular lattice strongly affects the ground state spin configuration when an antiferromagnetic coupling is present even though it is a short-range interaction. Indeed the ground state of the planar triangular model with NN antiferromagnetic exchange coupling is characterized by a *frustrated* 120° three-sublattice (T) configuration, whereas two-sublattice Néel long range order sets up in a square lattice. When the NN interaction is replaced by a competing interaction extended to next- (NNN) and third-nearest neighbors a variety of new configurations is found.[3] For short-range interaction any LRO at any finite temperature is prevented by the Mermin-Wagner theorem.[4] When a long-range antiferromagnetic interaction decaying as $1/r^3$ where r is the spin-spin distance is introduced no data about the ground state configuration or about the existence of LRO at finite temperature are available.

The aim of this paper is to investigate the ground state configuration and the thermal behavior of a planar triangular model with both dipole and isotropic long-range antiferromagnetic interactions. The study of a planar square model[2] with both dipole and long-range antiferromagnetic exchange interactions brings to an unexpected rich phase diagram. In terms of the parameter $\eta=\mu^2/a^3/(J_0+\mu^2/a^3)$, where $J_0>0$ is the isotropic antiferromagnetic interaction strength, μ is the magnetic moment, a is the lattice constant, different kinds of order are found. The zero temperature spin configuration is affected by continuous degeneracy. A four sublattice configuration in which the spins of an elmentary square make angles θ, $-\theta$, $\pi+\theta$, $\pi-\theta$ with a NN direction, θ being arbitrary, is stable for $0.210<\eta<1$ and a two-sublattice Néel configuration with the spins pointing along an arbitrary direction is stable for $0<\eta<0.210$. The continuous degeneracy is lifted by thermal fluctuations since the elementary excitation energy depends on the spin orientation with respect to the underlying lattice.

Low temperature expansion and Monte Carlo (MC) simulation lead to an even richer phase diagram for a triangular lattice. The main feature is the existence of striped configurations (AFn) of n rows of spins up and n rows of spin down pointing along a NN direction between the T configuration, stable for $0<\eta<0.086$ at zero temperature, and the F configuration, stable only for $\eta=1$ in the thermodynamic limit. The AF1 phase (corresponding to the C phase of the square lattice[2]) is stable in the large range $0.086<\eta<0.815$, but all AFn striped configurations are stable for smaller and smaller intervals of η, approaching the F configuration ($n\to\infty$). The continuous degeneracy of the F phase is lifted by thermal fluctuations and a next nearest neighbor (NNN) direction is selected. The phase transition to the paramagnetic phase is first order in contrast to the continuous phase transition found for the same model on the square lattice. Only for pure dipole interaction the phase transition is second order with the critical exponents that agree with the critical exponents of the square model.[2]

II. THE MODEL

The model Hamiltonian is

$$\mathcal{H}=-\frac{1}{2}\left(J_0+\frac{\mu^2}{a^3}\right)\sum_{\substack{i,\mathbf{r}\\ \mathbf{r}\neq 0}}\sum_{\alpha\beta} f^{\alpha\beta}(\mathbf{r})S_i^{\alpha}S_{i+\mathbf{r}}^{\beta}, \qquad (1)$$

where

$$f^{\alpha\beta}(\mathbf{r})=\frac{1}{r^3}\left(3\eta\frac{r^{\alpha}r^{\beta}}{r^2}-\delta_{\alpha,\beta}\right). \qquad (2)$$

i labels the $L\times L$ sites of a triangular lattice, $\mathbf{r}=l_1\mathbf{a}_1+l_2\mathbf{a}_2$ (with $\mathbf{a}_1=\mathbf{u}_x$ and $\mathbf{a}_2=1/2\mathbf{u}_x+\sqrt{3}/2\mathbf{u}_y$) joins the site i with a generic site of the lattice, α, β label the x,y components of the two-dimensional classical vector $\mathbf{S}_i$ located on the site i,

$\eta=\mu^2/a^3/(J_0+\mu^2/a^3)$ runs from 0 to 1 ($\eta=0$ corresponds to the pure antiferromagnetic case, $\eta=1$ corresponds to the pure dipole interaction). We assume that the ground state configuration of our model *may* be characterized by a regular helix so that we put

$$\mathbf{S_r}=S[\cos(\phi+\mathbf{Q}\cdot\mathbf{r}+\psi_\mathbf{r}),\sin(\phi+\mathbf{Q}\cdot\mathbf{r}+\psi_\mathbf{r})], \tag{3}$$

where $\mathbf{Q}$ is the pitch of the helix, ϕ is an arbitrary phase common to all spins of the lattice, $\psi_\mathbf{r}$ is a small deviation from the ground state configuration. At low temperature one can expand Hamiltonian (1) in terms of ψ and retain only bilinear contributions so obtaining

$$\mathcal{H}=E_0+\sum_\mathbf{q}\frac{1}{2}\left(J_0+\frac{\mu^2}{a^3}\right)S^2\lambda_\mathbf{q}\psi_\mathbf{q}\psi_{-\mathbf{q}}, \tag{4}$$

where

$$E_0=-\frac{1}{2}\left(J_0+\frac{\mu^2}{a^3}\right)S^2L^2\left\{[D^{xx}(\mathbf{Q})+D^{yy}(\mathbf{Q})]+\frac{1}{2}[D^{xx}(\mathbf{Q})-D^{yy}(\mathbf{Q})]\cos(2\phi)\,\delta_{2\mathbf{Q},\mathbf{G}}+D^{xy}(\mathbf{Q})\sin(2\phi)\,\delta_{2\mathbf{Q},\mathbf{G}}\right\}, \tag{5}$$

$$\begin{aligned}\lambda_\mathbf{q}=&\frac{1}{2}[D^{xx}(\mathbf{Q})-D^{yy}(\mathbf{Q})+D^{xx}(\mathbf{Q}-\mathbf{q})-D^{yy}(\mathbf{Q}-\mathbf{q})]\cos(2\phi)\,\delta_{2\mathbf{Q},\mathbf{G}}\\&+\frac{1}{2}[D^{xy}(\mathbf{Q})+D^{xy}(\mathbf{Q}-\mathbf{q})]\sin(2\phi)\,\delta_{2\mathbf{Q},\mathbf{G}}\\&+\frac{1}{2}\left\{D^{xx}(\mathbf{Q})-\frac{1}{2}[D^{xx}(\mathbf{Q}+\mathbf{q})+D^{xx}(\mathbf{Q}-\mathbf{q})]+D^{yy}(\mathbf{Q})-\frac{1}{2}[D^{yy}(\mathbf{Q}+\mathbf{q})+D^{yy}(\mathbf{Q}-\mathbf{q})]\right\}\end{aligned} \tag{6}$$

with

$$D^{\alpha\beta}(\mathbf{Q})=\sum_{\mathbf{r}\neq0}f^{\alpha\beta}(\mathbf{r})e^{i\mathbf{Q}\cdot\mathbf{r}}. \tag{7}$$

and $\psi_\mathbf{q}$ is the Fourier transform of $\psi_\mathbf{r}$. No linear term in $\psi_\mathbf{q}$ appears in Eq. (4) because its coefficient is proportional to the derivative of E_0 with respect to ϕ and we are only interested into the values of ϕ that minimize E_0. Note the discontinuity of the ground state energy for $\mathbf{Q}=\mathbf{G}/2$ where $\mathbf{G}=l_1\mathbf{a}_1^*+l_2\mathbf{a}_2^*$ [with $\mathbf{a}_1^*=2\pi(\mathbf{u}_x-1/\sqrt{3}\mathbf{u}_y)$ and $\mathbf{a}_2^*=4\pi/\sqrt{3}\mathbf{u}_y$] is a reciprocal lattice vector. We have investigated the ground state energy evaluating the lattice sum given by Eq. (7) as function of the wave vector $\mathbf{Q}$ for several values of η. No demagnetization factor is accounted for 2D systems because it vanishes as $1/L$ where L is the linear dimension of the sample in contrast to the 3D case where the demagnetization factor is finite for $L\to\infty$ and depends on the shape of the sample. We find that the minima of E_0 correspond to $\mathbf{Q}=\mathbf{Q}_F=0$ or $\mathbf{Q}=\mathbf{Q}_T=(1/3,2/3),(2/3,1/3),\ldots,$ or $\mathbf{Q}=\mathbf{Q}_C=(0,1/2),(1/2,0),(1/2,1/2),\ldots,$ depending on η. In particular we find $D^{xx}(\mathbf{Q}_F)=D^{yy}(\mathbf{Q}_F)=16.551\eta-11.034$ and $D^{xy}(\mathbf{Q}_F)=0$ in the ferromagnetic (F) configuration, $D^{xx}(\mathbf{Q}_T)=D^{yy}(\mathbf{Q}_T)=-3.498\eta+2.332$ and $D^{xy}(\mathbf{Q}_T)=0$ in the 120° three-sublattice (T) configuration, and $D^{xx}(\mathbf{Q}_C)=2.256\eta+1.839$, $D^{yy}(\mathbf{Q}_C)=-7.774\eta+1.839$, $D^{xy}(\mathbf{Q}_C)=0$ for $\mathbf{Q}_C=\mathbf{Q}_1=(0,1/2)$, $D^{xx}(\mathbf{Q}_C)=-5.266\eta+1.839$, $D^{yy}(\mathbf{Q}_C)=-0.251\eta+1.839$, $D^{xy}(\mathbf{Q}_C)=\mp4.343\eta$ for $\mathbf{Q}_C=\mathbf{Q}_2=(1/2,1/2)$ (upper sign) and $\mathbf{Q}_C=\mathbf{Q}_3=(1/2,0)$ (lower sign) in the collinear (C) configuration. For $0<\eta<0.086$ the ground state is

$$E_0(\mathbf{Q}_T)=-\frac{1}{2}\left(J_0+\frac{\mu^2}{a^3}\right)S^2L^2(-3.498\eta+2.332) \tag{8}$$

independent of ϕ. For $0.086<\eta<0.901$ the ground state is

$$E_0(\mathbf{Q}_C)=-\frac{1}{2}\left(J_0+\frac{\mu^2}{a^3}\right)S^2L^2(2.256\eta+1.839). \tag{9}$$

For $\mathbf{Q}_C=\mathbf{Q}_1,\mathbf{Q}_2,\mathbf{Q}_3$, one finds that the minimum corresponds to $\phi=0,2\pi/3,\pi/3$, respectively. The ground state energy of the C phase corresponds to alternating NN rows of parallel spins pointing along the rows. The discrete degeneracy is related to the three equivalent directions. Finally, for $0.901<\eta<1$ the ground state energy is

$$E_0(\mathbf{Q}_F)=-\frac{1}{2}\left(J_0+\frac{\mu^2}{a^3}\right)S^2L^2(16.551\eta-11.034) \tag{10}$$

and it is independent of ϕ. The ϕ independence of the ground state energy in the F and T phases implies the existence of a *continuous* degeneracy. The continuous degeneracy cannot be removed in the T phase within the harmonic approximation because in this case the ϕ dependence of the excitations energy as given in Eq. (6) disappears. On the contrary one expects that the continuous degeneracy is removed in the F phase. To see this we choose $\eta=1$ and evaluate the harmonic free energy

$$F=E_0-\frac{k_BTN}{2}\ln\left[\frac{k_BT}{2\pi(J_0+\mu^2/a^3)S^2}\right]+\frac{k_BT}{2}\sum_\mathbf{q}\ln(\lambda_\mathbf{q}). \tag{11}$$

We find that the free energy given by Eq. (11) is a periodic function of ϕ having minima at $\phi=\pi/6+k\pi/3$ corresponding to NNN directions and maxima in correspondence of $\phi=k\pi/3$ (NN directions). The breaking of the continuous degeneracy at finite temperature is the phenomenon of order by thermal disorder.[5] We think that the continuous degeneracy of the T phase for $\eta\neq0$ should be lifted going to higher order approximations since the dipole interaction breaks the continuous symmetry present only for $\eta=0$.

III. CHECK OF THE GROUND STATE

To test whether the hypothesis of a regular helix is correct we have performed analytic calculations assuming a triangu-

lar lattice divided into four and three sublattices. The four-sublattice assumption is consistent with the C and F phase, the three-sublattice one is consistent with the T and F configuration. This approach is very similar to the Luttinger-Tisza method[6] applied to square and cubic lattices.[7] The main advantage of this method is that no regular helix is assumed. The main disadvantage is that only magnetic cells with a small number of spins can be studied because of the rapid increasing of the matrix dimension.

For a cell with four spins the energy is given by

$$E_0=-\frac{L^2}{8}\left(J_0+\frac{\mu^2}{a^3}\right)(S_1^xS_2^xS_3^xS_4^xS_1^yS_2^yS_3^yS_4^y)\times\begin{pmatrix} W_{00}^{xx} & W_{10}^{xx} & W_{01}^{xx} & W_{01}^{xx} & 0 & 0 & -W_{01}^{xy} & W_{01}^{xy}\\ W_{10}^{xx} & W_{00}^{xx} & W_{01}^{xx} & W_{01}^{xx} & 0 & 0 & W_{01}^{xy} & -W_{01}^{xy}\\ W_{01}^{xx} & W_{01}^{xx} & W_{00}^{xx} & W_{10}^{xx} & -W_{01}^{xy} & W_{01}^{xy} & 0 & 0\\ W_{01}^{xx} & W_{01}^{xx} & W_{10}^{xx} & W_{00}^{xx} & W_{01}^{xy} & -W_{01}^{xy} & 0 & 0\\ 0 & 0 & -W_{01}^{xy} & W_{01}^{xy} & W_{00}^{xx} & W_{10}^{yy} & W_{01}^{yy} & W_{01}^{yy}\\ 0 & 0 & W_{01}^{xy} & -W_{01}^{xy} & W_{10}^{yy} & W_{00}^{xx} & W_{01}^{yy} & W_{01}^{yy}\\ -W_{01}^{xy} & W_{01}^{xy} & 0 & 0 & W_{01}^{yy} & W_{01}^{yy} & W_{00}^{xx} & W_{10}^{yy}\\ W_{01}^{xy} & -W_{01}^{xy} & 0 & 0 & W_{01}^{yy} & W_{01}^{yy} & W_{10}^{yy} & W_{00}^{xx}\end{pmatrix}\begin{pmatrix} S_1^x\\ S_2^x\\ S_3^x\\ S_4^x\\ S_1^y\\ S_2^y\\ S_3^y\\ S_4^y\end{pmatrix}, \tag{12}$$

where $W_{00}^{xx}=-1.379+2.068\eta$, $W_{10}^{xx}=-3.218+7.334\eta$, $W_{01}^{xx}=-3.218+3.573\eta$, $W_{10}^{yy}=-3.218+2.320\eta$, $W_{01}^{yy}=-3.218+6.081\eta$, $W_{01}^{xy}=2.171\eta$. The ground state energy is easily written in terms of the eigenvalues λ of the matrix given in Eq. (12)

$$E_0=-\frac{1}{2}\left(J_0+\frac{\mu^2}{a^3}\right)S^2L^2\lambda. \tag{13}$$

The eigenvalues are

$$\lambda_F=W_{00}^{xx}+W_{10}^{xx}+2W_{01}^{xx}=-11.034+16.551\eta \tag{14}$$

(ferromagnetic eigenvalue corresponding to a configuration with all spins parallel pointing in an arbitrary direction) twice degenerate,

$$\lambda_B=W_{00}^{xx}+W_{10}^{yy}-2W_{01}^{yy}=1.839-7.774\eta \tag{15}$$

(columnar phase corresponding to a configuration with spins pointing along the three equivalent NNN directions) three times degenerate,

$$\lambda_C=W_{00}^{xx}+W_{10}^{xx}-2W_{01}^{xx}=1.839+2.256\eta \tag{16}$$

(columnar phase corresponding to a configuration with spins pointing along the three equivalent NN directions) three times degenerate. The phase with spins pointing along NNN rows is never stable because $E_0(\lambda_B)>E_0(\lambda_C)$ for any η. The C phase is stable for $\eta<0.901$ and the ground state energy $E_0(\lambda_C)$ coincides with Eq. (9). For $\eta>0.901$ the F phase is stable with energy $E_0(\lambda_F)$ given by Eq. (10).

For a cell with three spins the energy reads

$$E_0=-\frac{L^2}{6}\left(J_0+\frac{\mu^2}{a^3}\right)(S_1^xS_2^xS_3^xS_1^yS_2^yS_3^y)\times\begin{pmatrix} W_{00}^{xx} & W_{10}^{xx} & W_{10}^{xx} & 0 & 0 & 0\\ W_{00}^{xx} & W_{10}^{xx} & W_{10}^{xx} & 0 & 0 & 0\\ W_{10}^{xx} & W_{00}^{xx} & W_{10}^{xx} & 0 & 0 & 0\\ 0 & 0 & 0 & W_{00}^{xx} & W_{10}^{xx} & W_{10}^{xx}\\ 0 & 0 & 0 & W_{10}^{xx} & W_{00}^{xx} & W_{10}^{xx}\\ 0 & 0 & 0 & W_{10}^{xx} & W_{10}^{xx} & W_{00}^{xx}\end{pmatrix}\begin{pmatrix} S_1^x\\ S_2^x\\ S_3^x\\ S_1^y\\ S_2^y\\ S_3^y\end{pmatrix}, \tag{17}$$

where $W_{00}^{xx}=-2.123+3.184\eta$, $W_{10}^{xx}=-4.455+6.682\eta$. The eigenvalues are

$$\lambda_F=W_{00}^{xx}+2W_{10}^{xx}=-11.034+16.551\eta \tag{18}$$

(ferromagnetic eigenvalue) twice degenerate, coincident with Eq. (14) and

$$\lambda_T=W_{00}^{xx}-W_{10}^{yy}=2.332-3.498\eta \tag{19}$$

(triangular phase) four times degenerate. Since $E_0(\lambda_T)<E_0(\lambda_F)$ for $\eta<2/3$ the T phase is stable in the range $0<\eta<2/3$ with energy given by Eq. (8). The spins make angles of $2\pi/3$ each other but any direction of the first spin may be chosen. It is interesting to note that the 120° helix is *not* distorted by the dipole anisotropic interaction. For $\eta>2/3$ the F phase is stable with energy given by Eq. (10). The continuous degeneracy is confirmed for both T and F phases.

At variance with the square planar model[2] the *C* phase does not show continuous degeneracy at $T=0$. For η increasing from pure isotropic antiferromagnetic interaction ($\eta=0$) to pure dipole interaction ($\eta=1$) *T*, *C*, and *F* phase are expected for the triangular lattice to be compared to the AF, *C*, *V*, *C* phase found in the square lattice.[2]

The spin waves of the *T* phase are well defined farther on the region of stability of the *T* phase ($0<\eta<0.086$). Indeed the stability region of spin waves is $0<\eta<2/3$. For $\eta=2/3$ the spectrum becomes very flat and the excitation energy very low. On the other hand the *C* phase is stable for $\eta>0.086$ so that the *T* configuration cannot affect the equilibrium properties of the model for such values of η. In conclusion the *T* phase is stable for $0<\eta<0.086$, *C* phase for $0.086<\eta<0.901$, and *F* phase for $0.901<\eta<1$. The present analysis confirms the ground state configurations and their stability range obtained in Sec. II where only regular helices have been considered.

An intriguing question arises about the spin wave spectrum in the *F* phase. Indeed except the case $\eta=1$ (pure dipole interaction) for any $0.901<\eta<1$ the spin wave spectrum is not well defined pointing out an instability of the ferromagnetic configuration.

IV. STRIPED CONFIGURATIONS

Striped phases (AF*n*) with *n* rows of spins up alternating with *n* rows of spins down are good candidates to connect the *C* phase (or AF1 configuration) with the *F* phase. Pure dipole interaction in the triangular lattice leads to *F* phase and pure isotropic antiferromagnetic interaction supports the *T* configuration. The hypothesis of a ground state configuration characterized by a regular helix or by a four spin magnetic cell leads to the AF1 configuration, but the possible existence of higher order striped phases has to be investigated by a direct calculation of the energy of these striped configurations.

The energy of a perfectly ordered striped configuration for an Ising model on a square lattice was evaluated taking NN ferromagnetic exchange and dipole interaction into account.[8] An analogous calculation for the Heisenberg model was performed in presence of uniaxial anisotropy.[9,10] We have extended this approach to the planar triangular model assuming the spins to point along the *x* axis, one of the three equivalent NN directions. For stripes of *n* rows the ground state energy is

$$E_0=-\frac{1}{2}\left(J_0+\frac{\mu^2}{a^3}\right)\sum_{\mathbf{q}} D^{xx}(\mathbf{q})S^x(\mathbf{q})S^x(-\mathbf{q})$$
$$=-\frac{1}{2}\left(J_0+\frac{\mu^2}{a^3}\right)S^2\sum_{\mathbf{q}} D^{xx}(\mathbf{q})\times\left(\frac{L}{n}\right)^2$$
$$\times\sum_{s}\ \delta_{q_x,0}\delta_{q_y,(4\pi/\sqrt{3}n)(s+1/2)}\frac{1}{\sin^2\left[\frac{\pi}{n}(s+1/2)\right]}, \tag{20}$$

TABLE I. Reduced ground state energy as function of η.

n	$E_0/[(J_0+\mu^2/a^3)L^2S^2]$	*n*	$E_0/[(J_0+\mu^2/a^3)L^2S^2]$
1	$-1.12794\eta-0.91951$	7	$-5.85273\eta+3.19513$
2	$-3.05887\eta+0.65364$	8	$-6.06700\eta+3.39679$
3	$-4.10732\eta+1.58432$	9	$-6.24287\eta+3.56284$
4	$-4.77422\eta+2.19234$	10	$-6.39013\eta+3.70225$
5	$-5.23966\eta+2.62245$	11	$-6.51544\eta+3.82114$
6	$-5.58505\eta+2.94428$	12	$-6.62353\eta+3.92387$

where *s* is an integer in the range $-(n+1)/2<s\leqslant(n-1)/2$ and

$$S^x(\mathbf{q})=\frac{1}{L}\sum_{m_1,m_2} S^x(m_1,m_2)e^{-iq_x(m_1+m_2/2)}e^{-iq_y(\sqrt{3}m_2/2)}. \tag{21}$$

For even *n* Eq. (20) becomes

$$E_0=-\left(J_0+\frac{\mu^2}{a^3}\right)L^2S^2\frac{1}{n^2}\sum_{s=0}^{(n-1)/2}\frac{D^{xx}\left(0,\frac{4\pi}{\sqrt{3}n}(s+1/2)\right)}{\sin^2\left[\frac{\pi}{n}(s+1/2)\right]}, \tag{22}$$

while for odd *n* Eq. (20) becomes

$$E_0=-\left(J_0+\frac{\mu^2}{a^3}\right)L^2S^2$$
$$\times\left[\frac{1}{n^2}\sum_{s=0}^{(n-1)/2}\frac{D^{xx}\left(0,\frac{4\pi}{\sqrt{3}n}(s+1/2)\right)}{\sin^2\left[\frac{\pi}{n}(s+1/2)\right]}-\frac{D^{xx}\left(0,\frac{2\pi}{\sqrt{3}}\right)}{2n^2}\right]. \tag{23}$$

In Table I we give the reduced ground state energy $E_0/[(J_0+\mu^2/a^3)L^2S^2]$ as function of η. In Table II the value of η at which the phase AF*n* is replaced by the phase AF($n+1$) is given for $1<n<11$. As one can see AF*n* phases with any *n* occur even though their range of stability becomes narrower and narrower for increasing *n*.

TABLE II. Values of η at which the phase AF*n* is replaced by the phase AF($n+1$).

n	η	*n*	η
1	0.81471	7	0.94111
2	0.88768	8	0.94419
3	0.91170	9	0.94668
4	0.92409	10	0.94874
5	0.93180	11	0.95047
6	0.93714		

TABLE III. Values of η at which the phase AFn set in for $L=24$.

	η
AF1-AF2	0.81471
AF2-AF3	0.88768
AF3-AF4	0.91170
AF4-AF6	0.92737
AF6-AF12	0.94329
AF12-F	0.96436

In order to find the ground state energy for large stripes ($n\to\infty$) an expansion of $D^{xx}(\mathbf{Q},\eta)$ for small $\mathbf{Q}$ is in order. Such an expansion, obtained in the Appendix, reads

$$D^{xx}\left(0,\frac{4\pi}{\sqrt{3}n}(s+1/2)\right) = 16.55126\eta - 11.03418 + \frac{4\pi}{\sqrt{3}}(1-\eta)\left[\frac{4\pi}{\sqrt{3}n}\left(s+\frac{1}{2}\right)\right] + (0.79002\eta - 1.05336)\left[\frac{4\pi}{\sqrt{3}n}\left(s+\frac{1}{2}\right)\right]^2 + \cdots. \quad (24)$$

Substitution of Eq. (24) into Eq. (22) gives the ground state energy of the striped phase for large n

$$E_0(n\to\infty) = -\left(J_0+\frac{\mu^2}{a^3}\right)L^2S^2\left\{8.27563\eta - 5.51709 + \frac{16\pi}{3}(1-\eta)\left[\frac{0.57893+(1/\pi)\ln n}{n}\right] + \frac{16}{3}(0.79002\eta - 1.05336)\frac{\ln 2}{n} + \cdots\right\}. \quad (25)$$

Note that $E_0(\infty)=E_F$ is the energy of the ferromagnetic F phase. In the thermodynamic limit the F phase is restricted to $\eta=1$ but for finite L the question about the stability of the F phase for $\eta\neq 1$ is still open. Indeed in a sample of $L\times L$ spins the last striped configuration appearing before the ferromagnetic one is characterized by $n=L/2$. Unfortunately the assumption of periodic boundary conditions, crucial to evaluate the expansion given in Eq. (24), prevents any application of Eq. (25) to sample in which the stripe width n is comparable with the sample size L. The finite size effect is expected to open a *finite* range of stability of the F phase, which shrinks to a point in the thermodynamic limit ($L\to\infty$). If it was not so, it should become hard to explain the ferromagnetic phase with spins out-of-plane observed in epitaxial films of transition metals grown on gold, silver or copper substrates.[11,12]

In Table III we give the values of η for which the AFn phases are stable for $L=24$, a lattice size chosen for the most part of MC simulation of the next section. As one can see only a few AFn phases survive (i.e., AF1, AF2, AF3, AF4, AF6, and AF12): the only striped phases that satisfy the periodic boundary conditions.

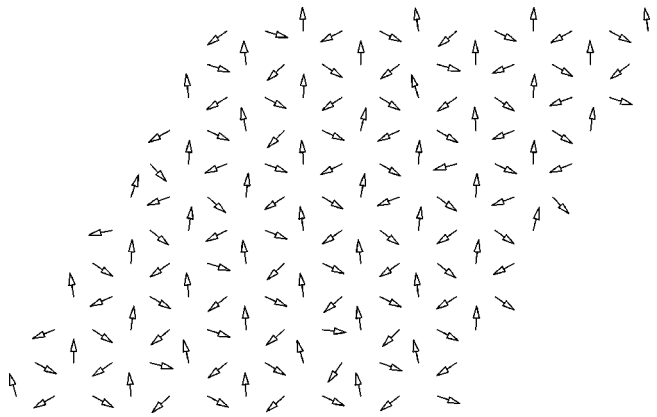

FIG. 1. Snapshots of a triangular lattice of 12×12 spins obtained from MC simulation for $T=0.02$ and $\eta=0.05$ after 10^5 MCS from a random configuration.

The planar model involves two-component spin vectors but it falls in the same class of symmetry of the Heisenberg model with easy-plane anisotropy so that the ground state configurations we find are the ground state configurations for a relevant set of three-component spin models. Note that the lattice structure, the long-range character of the exchange interaction, and the easy-plane nature of the anisotropic long-range dipole interaction are essential to get striped phases with in-plane spin configurations. Indeed all models previously considered concerning a square lattice with uniaxial (Ising-like) anisotropy, NN exchange interaction, and dipole interaction led to strip domains with only out-of-plane spin configurations.[9,10] On the other hand in-plane strip domains were observed in ultrathin films of Co layers on Au substrate[11] when the dipole interaction dominates the uniaxial surface anisotropy, that is when the film thickness reaches a critical number of monolayers. An analogous behavior was observed in Fe layers on Cu substrate[12] where the onset of out-of-plane and in-plane striped configurations at increasing the film thickness or the temperature is even more impressive.

V. MONTE CARLO SIMULATION

We have performed Monte Carlo (MC) simulations on $L\times L$ triangular lattices with $L=12$, 18, 24, 36 following the periodic ''images'' approach.[13] Low temperature MC simulations confirm the kind of order expected on the basis of analytic calculations of Secs. II and IV. In Fig. 1 a snapshot of a 12×12 triangular lattice is shown for $\eta=0.05$ (T phase) at $T=0.02$ where the temperature is in units $(J_0+\mu^2/a^3)S^2$. In Fig. 2 the snapshot is taken at the same temperature for $\eta=0.5$ (AF1 phase). In Fig. 3 the snapshot is shown for $\eta=0.85$ (AF2 phase) at $T=0.03$. The snapshots are taken after 10^5 MC steps for the T and AF1 phase and after 10^6 MC steps for the AF2 phase starting from a random configuration. Higher order striped configurations have energies so close and stability regions so narrow that the MC

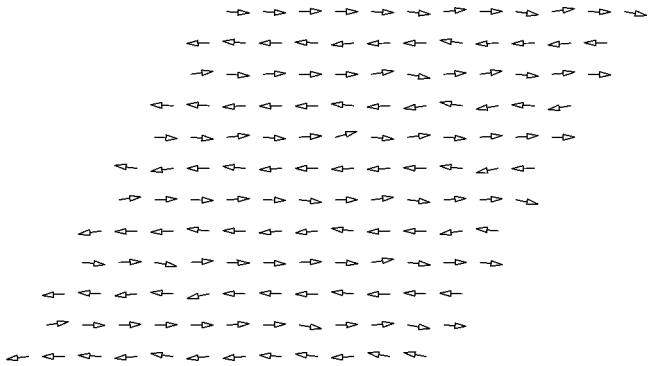

FIG. 2. Snapshots of a triangular lattice of 12×12 spins obtained from MC simulation for $T=0.02$ and $\eta=0.5$ after 10^5 MCS from a random configuration.

simulation calls for longer and longer computing time to pick out the configuration expected on the basis of the ground state energy calculation. For instance, the AF3 phase, expected for $\eta=0.9$ (see Table III), is seen in a long MC simulation but occasionally also the AF4 phase appears. Snapshots of AF1 and AF2 configurations with the spins pointing along the other two equivalent NN directions as well as snapshots of the F phase configuration for $\eta=1$ with spins pointing along any NNN direction have been recorded in other MC runs.

In Fig. 4 we show the phase diagram obtained by MC simulation on a 24×24 lattice. The phase transition to the disordered (paramagnetic) P phase has been located looking at the peak of the specific heat

$$c=\beta^2(\langle\mathcal{H}^2\rangle-\langle\mathcal{H}\rangle^2)/L^2, \tag{26}$$

and of the staggered susceptibility

$$\chi(\mathbf{Q})=(\langle|\mathbf{M}|^2\rangle-\langle|\mathbf{M}|\rangle^2)/L^2, \tag{27}$$

where $\mathbf{M}=\Sigma_{\mathbf{r}}e^{i\mathbf{Q}\cdot\mathbf{r}}\mathbf{S}_{\mathbf{r}}$ and $\mathbf{Q}=\mathbf{Q}_T,\mathbf{Q}_C,\mathbf{Q}_F$, for T, AF1, and F phase, respectively. Simulations are performed averaging over eight independent MC runs. In each run 10^4 configurations over 10^5 MC steps are accounted for, 10^3 are discarded for thermalization assuming as starting configuration the final configuration of the previous temperature. This implies that a very long effective simulation is performed for temperatures in the critical region. At zero temperature the T, AFn (with $n=1,2,3,4,6,12$), and F configurations are obtained by analytic calculations as shown in Table III. MC simulations recover the T, AFn (with $n=1,2,3$), and F configurations unambiguously while the identification of the AFn configurations with $n\geq4$ is very delicate.

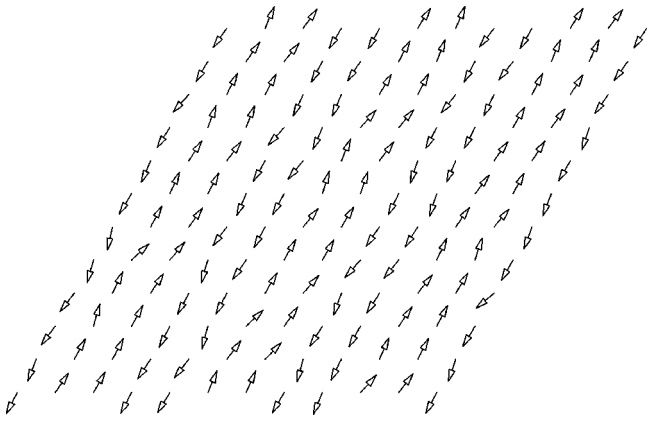

FIG. 3. Snapshots of a triangular lattice of 12×12 spins obtained from MC simulation for $T=0.03$ and $\eta=0.85$ after 10^6 MCS from a random configuration.

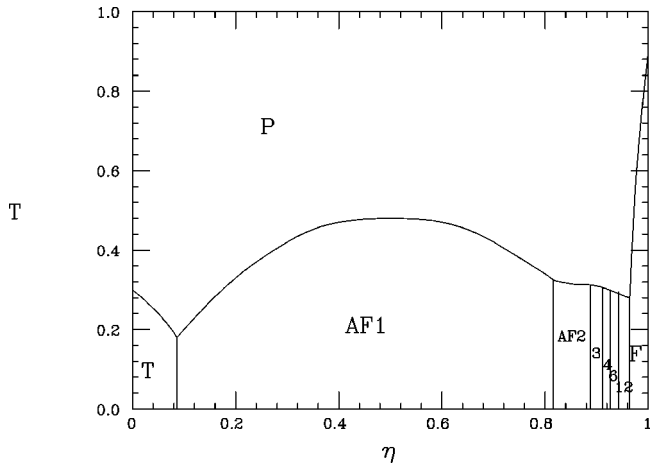

FIG. 4. Phase diagram of the planar triangular model as obtained from MC simulation on a 24×24 lattice. $T,P,F,$AFn mean 120° three-sublattice, paramagnetic, ferromagnetic, striped antiferromagnetic phase, n being the stripe width.

In Figs. 5, 6, 7 the specific heat, the staggered susceptibility and the order parameter

$$\psi=\langle|\mathbf{M}|\rangle/L^2 \tag{28}$$

are shown versus temperature for $\eta=1$ (F phase). The size scaling indicates the existence of a continuous phase transition at $T_c=0.88$. We find that $\nu=1$ is consistent with the size scaling of the temperature at which the susceptibility reaches its maximum. We obtain $\gamma=1.70\pm0.03$ and $\beta=0.21\pm0.03$ in agreement with the correspondent critical exponents obtained for the square model.[2] We have tested the

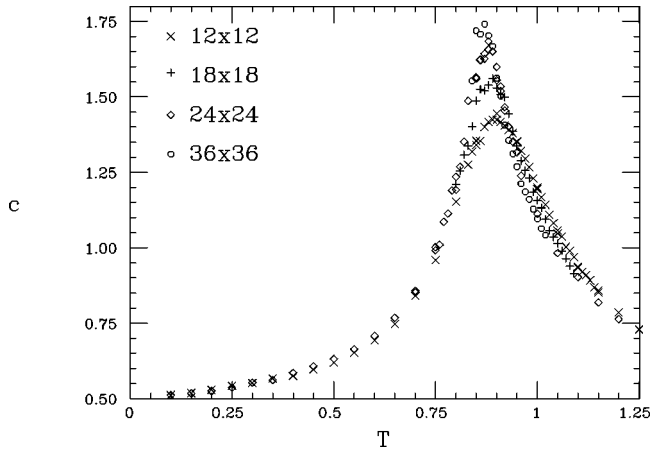

FIG. 5. Specific heat c versus reduced temperature T for several lattice sizes as obtained from MC simulation. $L=12$ (crosses), $L=18$ (vertical crosses), $L=24$ (diamonds), $L=36$ (circles).

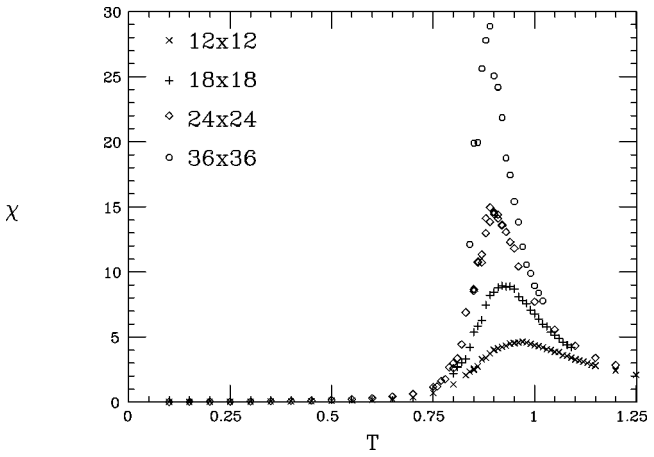

FIG. 6. Susceptibility $\chi=\chi(\mathbf{Q}=0)$ versus reduced temperature T for several lattice sizes as obtained from MC simulation. $L=12$ (crosses), $L=18$ (vertical crosses), $L=24$ (diamonds), $L=36$ (circles).

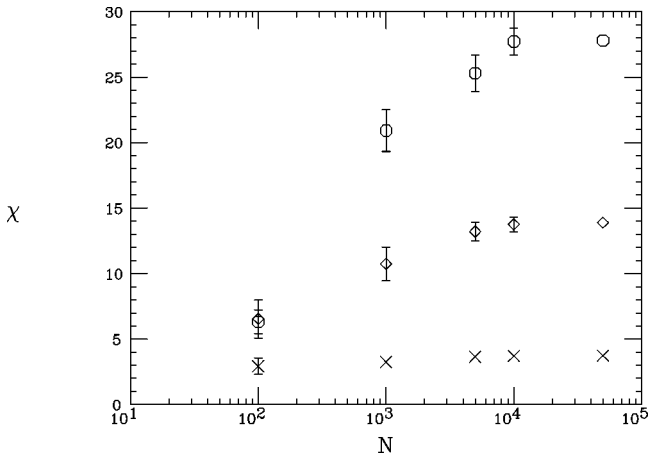

FIG. 8. Sucseptibility for $\eta=1$ at $T=0.89$ for samples of size 12×12 (crosses), 24×24 (diamonds), and 36×36 (circles) as a functiion of N where N is the number of configurations taken in the MC average. We have omitted the vertical error bars when smaller than the size of data points.

reliability of our MC data evaluating the susceptibility for $\eta=1$ at the transition temperature as function of the number of MC steps starting from the ground state configuration as suggested by Ferrenberg *et al.*[14] In Fig. 8 the susceptibility is shown as function of N where N is the number of spin configurations used to evaluate the MC average. Each configuration is taken every 10 MC steps. All data points of Fig. 8 are obtained by an average over 8 independent MC runs. The asymptotic values of χ_L for different lattice size as obtained by the plateau of Fig. 8 are $\chi_{12}\simeq3.5,\chi_{24}\simeq14,\chi_{36}\simeq28$ which agree with the maximum values of χ shown in Fig. 6. This is a strong indication that our MC simulations describe correctly the thermal equilibrium behavior of the model.

In the triangular lattice the point $\eta=1$ appears to be very peculiar. Indeed we have found that the elementary excitation spectrum is unstable for any $\eta\neq1$ in the thermodynamic limit. On the other hand the order parameter for $\eta\neq1$ falls off abruptly at the transition temperature suggesting the occurrence of a possible first order phase transition. To get unambiguous identification of the order of the phase transition we have followed the approach developed by Challa *et al.*[15] This approach was applied to the 2D ten-state Potts model which is known to have a first order phase transition[16] to assess the accuracy of the method. Indeed the time dependent behavior of the internal energy and of the order parameter near the transition temperature points out the phase coexistence. A two-peak structure of the probability distribution of the internal energy $P(E)$ and of the order parameter $P(\psi)$ at the transition temperature is a signature of a first order phase transition.

Figure 9 shows the reduced internal energy E measured in $(J_0+\mu^2/a^3)S^2L^2$ units and the order parameter ψ for $\eta=0.85$ (AF1 phase) versus time in MC simulation on a 24

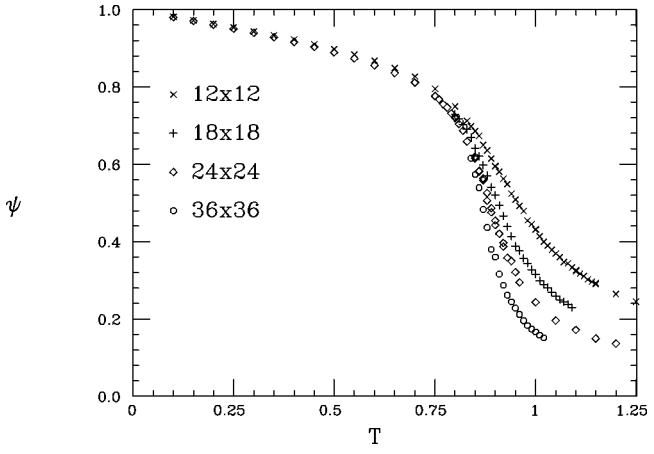

FIG. 7. Order parameter ψ versus reduced temperature T for several lattice sizes as obtained from MC simulation. $L=12$ (crosses), $L=18$ (vertical crosses), $L=24$ (diamonds), $L=36$ (circles).

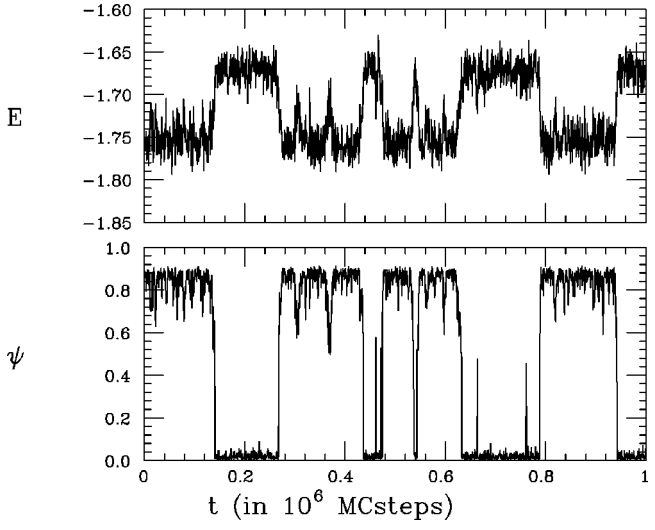

FIG. 9. Reduced internal energy E (upper panel) and order parameter ψ (lower panel) versus time in MC simulations on a 24 $\times24$ lattice at $T=0.32$ for $\eta=0.85$. The instantaneous values of E and ψ are plotted after every 500 MC steps.

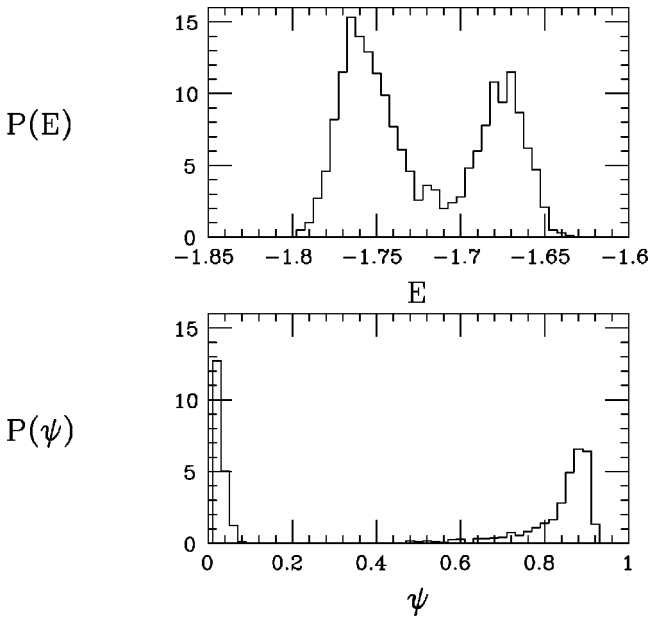

FIG. 10. Probability distribution of the reduced internal energy E (upper panel) and of the order parameter ψ (lower panel) in MC simulations on a 24×24 lattice at $T=0.32$ for $\eta=0.85$.

$\times 24$ lattice at $T=0.32$. The instantaneous values of E and ψ are plotted after every 500 MC steps. In spite of the smallness of the latent heat $E_P-E_{\mathrm{AF2}}=0.12$, the coexistence of the AF2 configuration and of the P (paramagnetic) phase is clearly pointed out. $P(E)$ and $P(\psi)$ are shown in Fig. 10 as obtained by MC simulation on a 24×24 lattice at $T=0.32$

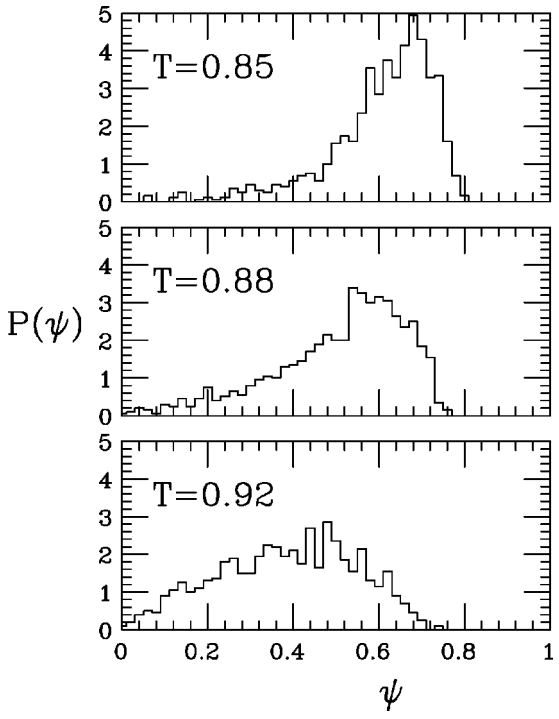

FIG. 11. Probability distribution of the order parameter ψ in MC simulations on a 24×24 lattice at temperatures about the critical temperature ($T=0.88$) for $\eta=1$.

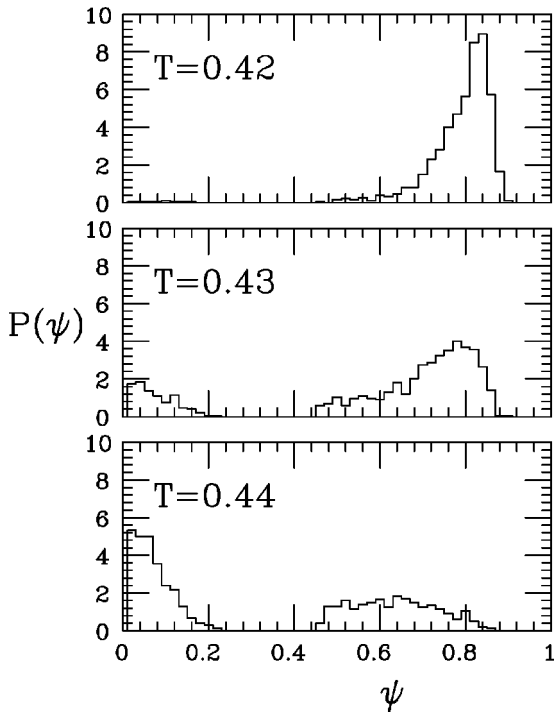

FIG. 12. Probability distribution of the order parameter ψ in MC simulations on a 24×24 lattice at temperatures about the first order transition temperature ($T=0.435$) for $\eta=0.7$.

for $\eta=0.85$. The two-peak structure is clearly seen. Note that only one peak in the probability distribution survives when the temperature is slightly changed to $T=0.32\pm\Delta T$ with $\Delta T=0.005$. The single peak below and above the transition temperature corresponds to the homogeneous ordered and disordered phase, respectively.

For comparison in Fig. 11 the probability distribution of the order parameter is shown for $\eta=1$ where the phase transition is continuous. Always one peak is present moving about the transition temperature $T_c=0.88$. The continuous character of the transition for $\eta=1$ is consistent with the above analysis of critical exponents. In Fig. 12 $P(\psi)$ is shown for $\eta=0.7$ where AF1 phase is stable. The two-peak structure is present near the first order transition temperature $T=0.435$ whereas only a single peak appears in the ordered phase at $T=0.42$. Incidentally, for this value of η the latent heat is so small that $P(E)$ shows a single (broad) peak structure that can be explained by the overlap of two peaks too close to be resolved. The same behavior is found for any $\eta<0.7$. For comparison the probability distribution of the reduced internal energy $P(E)$ and of the order parameter $P(\psi)$ is shown in Fig. 13 for $\eta=0.1$ at the transition temperature $T=0.21$ as obtained by MC simulation on a 24×24 lattice. As one can see the two-peak structure is clearly seen in $P(\psi)$ (lower panel). On the contrary only a single broad peak is seen in $P(E)$ (upper panel) because the two peaks centered at the internal energy of the AF1 and of the P phase are so close that they cannot be resolved. This fact leads to the conclusion that the latent heat of this ''weak'' first order phase transition is very small.

In a first order phase transition the maximum of the spe-

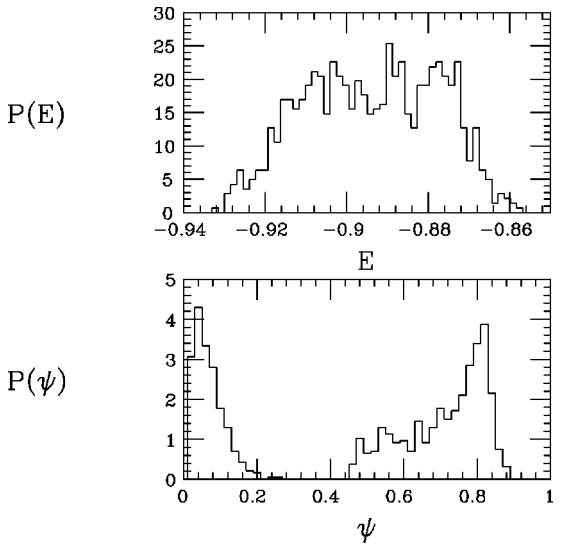

FIG. 13. Probability distribution of the reduced internal energy E (upper panel) and of the order parameter ψ (lower panel) in MC simulations on a 24×24 lattice at $T=0.21$ for $\eta=0.1$.

cific heat grows as L^d where d is the dimensionality of the model and L is the size of the sample.[15] Such a behavior can be obtained by inspection of Fig. 14 (left panel) for $\eta=0.8$ where the ordered phase is AF1. Indeed the maximum of the specific heat scales by a factor 4 going from $L=12$ to $L=24$ and by a factor 9 going from $L=12$ to $L=36$ as expected from the size scaling $c\sim L^2$ when a first order phase transition occurs. In the right panel of Fig. 14 the order parameter versus temperature is shown for $\eta=0.8$ and $L=24$. As one can see the disappearance of LRO occurs abruptly. Note that at the transition temperature $T=0.315$ we have quoted two data points corresponding to $\psi=0.86$ (ordered phase AF1) and to $\psi=0.02$ (paramagnetic phase). Indeed 5892 MC configurations contribute to the first value, 4108 to the second over 10^4 MC configurations selected for

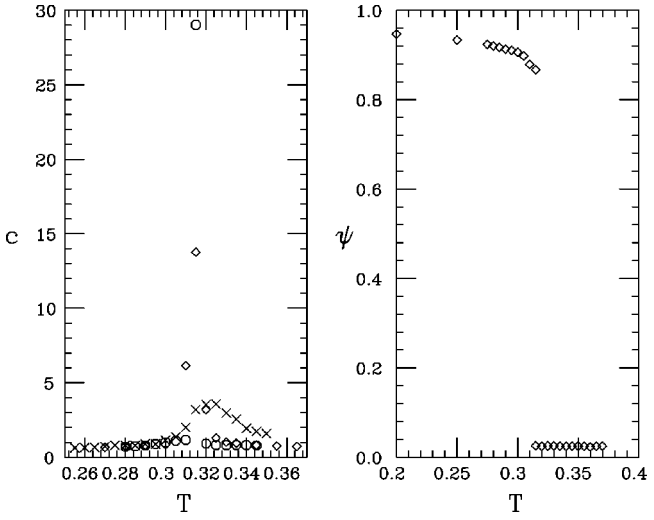

FIG. 14. Specific heat (left panel) and order parameter (right panel) versus temperature for $\eta=0.8$ in MC simulations on lattices of size 12×12 (crosses), 24×24 (diamonds), 36×36 (circles).

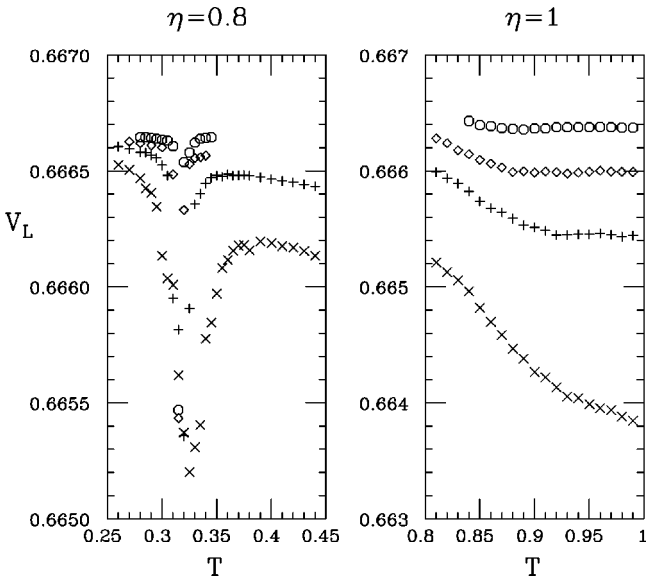

FIG. 15. Fourth order cumulant coefficient V_L as obtained from MC simulations on sample of different lattice size [12×12 (crosses), 18×18 (vertical crosses), 24×24 (diamonds), 36×36 (circles)] for $\eta=0.8$ (left panel) and for $\eta=1$ (right panel).

the thermal average. Note that 9914 MC configurations contribute to the value $\psi=0.87$ at $T=0.31$, while the total of MC configurations lead to $\psi=0.02$ at $T=0.32$. Even though a naive average of the data was taken at $T=0.315$, leading to $\psi=0.51$, an abrupt fall of the order parameter (instead of a discontinuity) should have been found giving a strong indication of a discontinuous phase transition.

An additional support to the first order character of the transition is provided by the fourth order cumulant

$$V_L=1-\frac{\langle\mathcal{H}^4\rangle_L}{3\langle\mathcal{H}^2\rangle_L} \tag{29}$$

which shows a very different temperature variation depending on the order of the phase transition. A pronounced minimum appears at a first order phase transition whereas V_L is temperature independent with constant value 2/3 for $L\to\infty$, when a continuous phase transition occurs.[15] Figure 15 shows V_L for $\eta=0.8$ as obtained by MC simulation for $L=12$, 18, 24, 36. The minimum and its narrowing at increasing L is clearly seen as expected[15] for a first order phase transition (left panel). Under the hypothesis that the phase coexistence can be described by a superposition of two Gaussians centered at the internal energies of the ordered and disordered phase, E_{AF1} and E_{P}, respectively, the value of the minimum of V_L can be deduced in thermodynamic limit[15]

$$V_L|_{\min}=1-\frac{[E_P^2+E_{\mathrm{AF1}}^2]^2}{12E_P^2E_{\mathrm{AF1}}^2}. \tag{30}$$

For $\eta=0.8$ we obtain $E_P=-1.52$ and $E_{\mathrm{AF1}}=-1.63$ at $T=0.32$ by MC simulation on a 24×24 lattice. Inserting these data in Eq. (30) one obtains $V_L|_{\min}=0.6653$ in good agreement with the minimum of Fig. 15 (left panel). In the right panel of Fig. 15 the thermal variation of V_L is shown for η

$=1$ where the phase transition is continuous. No minimum is present and the expected value 2/3 is approached increasing the lattice size.

VI. SUMMARY AND CONCLUSIONS

The triangular planar model is considered when both isotropic antiferromagnetic long-range exchange interaction decaying as $1/r^3$ and anisotropic dipole intraction are present. Ground state configuration and elementary excitation energy are obtained analytically while thermal behavior (i.e., specific heat, staggered susceptibility, and order parameter) is studied at any temperature by MC simulation for any value of η, between $\eta=0$ (pure isotropic antiferromagnetic interaction) and $\eta=1$ (pure dipole interaction). The phase diagram in the plane (η,T) is shown in Fig. 4 for a 24×24 sample which shows the qualitative features of the phase diagram for a generic *L*. *T*, AF*n* ($n=1,2,3,\ldots$), and *F* ordered phases are found. It is worthwile to compare this phase diagram with that obtained for the same model on a square lattice shown in Fig. 13 of Ref. 2. The *T* phase replaces the AF phase, AF1 is the same as the *C* phase, but the AF*n* configurations with $n\geqslant2$ have not equivalent counterpart in a square lattice, where, on the other hand, a vortical (*V*) phase was found. Finally, for $\eta=1$ *F* phase occurs instead of the *C* phase of the square lattice. At zero temperature the continuous degeneracy affects the *T* and *F* phase, not the AF*n* phases at variance with the square planar model where the continuous degeneracy is present for any η. Another impressive difference entered by the close packed nature of lattice is that the order-disorder phase transition is first order except for $\eta=1$ where it is second order. On the contrary in the square lattice the transition to the paramagnetic phase is continuous for any value of η. For $\eta=1$ size scaling analysis of susceptibility and order parameter gives the same critical exponents for the *F*-*P* transition in the triangular model as for the *C*-*P* transition in the square model.

The in-plane striped AF*n* configurations are a novelty of our model with respect to similar models where a short range exchange interaction was considered[8–10] and only strip domains with out of-plane spin configurations were found when a sufficient uniaxial Ising-like anisotropy was introduced. Note that no difference exists between the planar model and the classical Heisenberg model as for ground state configurations because of the role of the dipole interaction that acts as an easy-plane anisotropy favoring the in-plane spin configurations. In-plane strip domains were observed experimentally in ultrathin films of Co layers on Au substrate[11] and of Fe layers on Cu substrate.[12] Similar phases are found in the planar triangular model with long-range isotropic antiferromagnetic interaction along with anisotropic dipole interaction.

APPENDIX

The Appendix illustrates a method to perform a small-**Q** expansion of

$$D^{xx}(\mathbf{Q},\eta)=\sum_{\mathbf{r}\neq0}\frac{e^{i\mathbf{Q}\cdot\mathbf{r}}}{r^3}\left[3\eta\left(\frac{r_x}{r}\right)^2-1\right], \tag{A1}$$

where **r** is a dimensionless lattice vector. Consider the identities

$$\sum_{\mathbf{r}\neq0}\frac{e^{i\mathbf{Q}\cdot\mathbf{r}}}{r^5}=\frac{8}{3\sqrt{\pi}}\sum_{\mathbf{r}\neq0}e^{i\mathbf{Q}\cdot\mathbf{r}}\int_0^\infty dz z^4e^{-r^2z^2}, \tag{A2}$$

$$\sum_{\mathbf{r}\neq0}\frac{e^{i\mathbf{Q}\cdot\mathbf{r}}}{r^3}=\frac{4}{\sqrt{\pi}}\sum_{\mathbf{r}\neq0}e^{i\mathbf{Q}\cdot\mathbf{r}}\int_0^\infty dz z^2e^{-r^2z^2}, \tag{A3}$$

$$\sum_{\mathbf{r}\neq0}\frac{r_x^2}{r^5}e^{i\mathbf{Q}\cdot\mathbf{r}}=-\frac{\partial^2}{\partial Q_x^2}\sum_{\mathbf{r}\neq0}\frac{e^{i\mathbf{Q}\cdot\mathbf{r}}}{r^5}. \tag{A4}$$

Split integrals appear in Eqs. (A2) and (A3) as follows

$$\int_0^\infty dz z^pe^{-r^2z^2}=\int_0^\alpha dz z^pe^{-r^2z^2}+\int_\alpha^\infty dz z^pe^{-r^2z^2}. \tag{A5}$$

The second integral can be easily expressed in terms of the complementary error function $\mathrm{erfc}(x)=2/\sqrt{\pi}\int_x^\infty e^{-t^2}dt$ giving

$$\int_\alpha^\infty dz z^pe^{-r^2z^2}=\frac{1}{r^{p+1}}F_p(\alpha r), \tag{A6}$$

where

$$F_2(x)=\frac{1}{2}xe^{-x^2}+\frac{\sqrt{\pi}}{4}\mathrm{erfc}(x) \tag{A7}$$

and

$$F_4(x)=\frac{1}{2}x\left(\frac{3}{2}+x^2\right)e^{-x^2}+\frac{3\sqrt{\pi}}{8}\mathrm{erfc}(x). \tag{A8}$$

As for the first integral appearing in Eq. (A5) it is more convenient to transform before the sum over lattice vectors **r** appearing in Eqs. (A2) and (A3) into a sum over reciprocal lattice vectors **G** according to the equality[17]

$$\frac{1}{\pi}\sum_{\mathbf{r}}s^2e^{-s^2r^2+i\mathbf{Q}\cdot\mathbf{r}}=\rho\sum_{\mathbf{G}}e^{-|\mathbf{Q}+\mathbf{G}|^2/4s^2} \tag{A9}$$

where $\rho=2/\sqrt{3}$ for the triangular lattice. This gives

$$\sum_{\mathbf{r}\neq0}e^{i\mathbf{Q}\cdot\mathbf{r}}\int_0^\alpha dz z^pe^{-r^2z^2}=\pi\rho\alpha^{p-1}\sum_{\mathbf{G}}f_p\left(\frac{|\mathbf{Q}+\mathbf{G}|}{2\alpha}\right)-\frac{\alpha^{p+1}}{p+1}, \tag{A10}$$

where

$$f_2(x)=e^{-x^2}-\sqrt{\pi}x\,\mathrm{erfc}(x) \tag{A11}$$

and

$$f_4(x)=\frac{1-2x^2}{3}e^{-x^2}+\frac{2}{3}\sqrt{\pi}x^3\ \mathrm{erfc}(x). \tag{A12}$$

By use of Eqs. (A6) and (A10), Eqs. (A3) and (A4) become

$$\sum_{\mathbf{r}\neq 0}\frac{e^{i\mathbf{Q}\cdot\mathbf{r}}}{r^3}=\frac{4}{\sqrt{\pi}}\sum_{\mathbf{r}\neq 0}e^{i\mathbf{Q}\cdot\mathbf{r}}\frac{1}{r^3}F_2(\alpha r)+\frac{4}{\sqrt{\pi}}\left[\pi\rho\alpha\sum_{\mathbf{G}}f_2\left(\frac{|\mathbf{Q}+\mathbf{G}_l|}{2\alpha}\right)-\frac{1}{3}\alpha^3\right] \tag{A13}$$

and

$$\sum_{\mathbf{r}\neq 0}\frac{r_x^2}{r^5}e^{i\mathbf{Q}\cdot\mathbf{r}}=\frac{8}{3\sqrt{\pi}}\sum_{\mathbf{r}\neq 0}e^{i\mathbf{Q}\cdot\mathbf{r}}\frac{(r_x)^2}{r^5}F_4(\alpha r)+\frac{8}{3\sqrt{\pi}}\pi\rho\alpha^3\times\sum_{\mathbf{G}}\left[\frac{1}{2\alpha^2}e^{-|\mathbf{Q}+\mathbf{G}|^2/4\alpha^2}-\frac{\sqrt{\pi}}{4\alpha^3}\times\left(|\mathbf{Q}+\mathbf{G}|+\frac{(Q_x+G_x)^2}{|\mathbf{Q}+\mathbf{G}|}\right)\mathrm{erfc}\left(\frac{|\mathbf{Q}+\mathbf{G}|}{2\alpha}\right)\right]. \tag{A14}$$

Using Eqs. (A13) and (A14), Eq. (A1) becomes

$$D^{xx}(\mathbf{Q},\eta)=\frac{4\alpha^3}{3\sqrt{\pi}}-\frac{8\alpha\sqrt{\pi}}{\sqrt{3}}(1-\eta)\sum_{\mathbf{G}}f_2\left(\frac{|\mathbf{Q}+\mathbf{G}|}{2\alpha}\right)-\frac{4\pi\eta}{\sqrt{3}}\sum_{\mathbf{G}}\frac{(Q_x+G_x)^2}{|\mathbf{Q}+\mathbf{G}|}\mathrm{erfc}\left(\frac{|\mathbf{Q}+\mathbf{G}|}{2\alpha}\right)+\frac{8\eta}{\sqrt{\pi}}\sum_{\mathbf{r}\neq 0}e^{i\mathbf{Q}\cdot\mathbf{r}}\frac{r_x^2}{r^5}F_4(\alpha r)-\frac{4}{\sqrt{\pi}}\sum_{\mathbf{r}\neq 0}e^{i\mathbf{Q}\cdot\mathbf{r}}\frac{1}{r^3}F_2(\alpha r). \tag{A15}$$

Expansion of Eq. (A15) for $Q_x=0$, $Q_y\to 0$ gives

$$D^{xx}(Q_x=0,Q_y\to 0,\eta)=D_0^{xx}(\eta)+D_1^{xx}(\eta)|Q_y|+D_2^{xx}(\eta)Q_y^2+\cdots, \tag{A16}$$

where

$$D_0^{xx}(\eta)=\frac{4\alpha^3}{3\sqrt{\pi}}-\frac{8\alpha\sqrt{\pi}}{\sqrt{3}}(1-\eta)\sum_{\mathbf{G}}f_2\left(\frac{|\mathbf{G}|}{2\alpha}\right)-\frac{4\pi\eta}{\sqrt{3}}\sum_{\mathbf{G}\neq 0}\frac{G_x^2}{G}\mathrm{erfc}\left(\frac{G}{2\alpha}\right)+\frac{8\eta}{\sqrt{\pi}}\sum_{\mathbf{r}\neq 0}\frac{r_x^2}{r^5}F_4(\alpha r)-\frac{4}{\sqrt{\pi}}\sum_{\mathbf{r}\neq 0}\frac{1}{r^3}F_2(\alpha r), \tag{A17}$$

$$D_1^{xx}(\eta)=\frac{4\pi}{\sqrt{3}}(1-\eta), \tag{A18}$$

$$D_2^{xx}(\eta)=\frac{2\sqrt{\pi}}{\alpha\sqrt{3}}(1-\eta)\left\{1+\sum_{\mathbf{G}\neq 0}\left[\frac{G_y^2}{G^2}e^{-G^2/4\alpha^2}-\alpha\sqrt{\pi}\frac{G_x^2}{G^3}\mathrm{erfc}\left(\frac{G}{2\alpha}\right)\right]\right\}-\frac{\sqrt{\pi}}{\alpha^3\sqrt{3}}\eta\sum_{\mathbf{G}\neq 0}\frac{G_x^2}{G^4}\times e^{-G^2/4\alpha^2}[6\alpha^2G_y^2+G^2(G_y^2-2\alpha^2)]-\frac{2\pi}{\sqrt{3}}\eta\sum_{\mathbf{G}\neq 0}\frac{G_x^2}{G^5}(2G_y^2-G_x^2)\mathrm{erfc}\left(\frac{G}{2\alpha}\right)-\frac{4\alpha}{\sqrt{\pi}}\sum_{\mathbf{r}\neq 0}\frac{r_x^2r_y^2}{r^5}F_4(\alpha r)+\frac{2}{\sqrt{\pi}}\sum_{\mathbf{r}\neq 0}\frac{r_y^2}{r^3}F_2(\alpha r). \tag{A19}$$

Note that the nonanalytic term linear in the wave vector disappears when the pure dipole interaction is accounted for ($\eta=1$). Numerical evaluation of Eqs. (A17), (A19) can be performed taking $\alpha=2$ and restricting the rapidly convergent sums over few lattice vectors and reciprocal lattice vectors.[17] The result is

$$D_0^{xx}(\eta)=-11.03417574+16.55126360\eta,$$
$$D_2^{xx}(\eta)=-1.053355659+0.790016744\eta. \tag{A20}$$

*Also at Istituto IMEM del CNR, Parco Area delle Scienze, 43100 Parma, Italy. Electronic address: rastelli@fis. unipr. it

[1] M. Baher, M. Winkelmann, P. Vorderwisch, M. Steiner, C. Pich and F. Schwabl, Phys. Rev. B **54**, 12932 (1996).
[2] E. Rastelli, S. Regina, A. Tassi, and A. Carbognani, Phys. Rev. B **65**, 094412 (2002).
[3] E. Rastelli, A. Tassi, and L. Reatto, J. Magn. Magn. Mater. **15-18**, 357 (1980).
[4] N.D. Mermin and H. Wagner, Phys. Rev. Lett. **17**, 1133 (1966).
[5] J. Villain, R. Bideaux, J.P. Carton, and R. Conte, J. Phys. (France) **41**, 1263 (1980).
[6] J.M. Luttinger and L. Tisza, Phys. Rev. **70**, 954 (1946).
[7] P.I. Belobrov, R.S. Gekht, and V.A. Ignatchenko, Sov. Phys. JETP **57**, 636 (1983).
[8] A.B. MacIsaac, J.P. Whitehead, M.C. Robinson, and K. De'Bell, Phys. Rev. B **51**, 16033 (1995).
[9] M.B. Taylor and B.L. Gyorffy, J. Phys.: Condens. Matter **5**, 4527 (1993).
[10] A.B. MacIsaac, K. De'Bell, and J.P. Whitehead, Phys. Rev. Lett. **80**, 616 (1998).
[11] R. Allenspach, M. Stampanoni, and A. Bischof, Phys. Rev. Lett. **65**, 3344 (1990).
[12] R. Allenspach and A. Bischof, Phys. Rev. Lett. **69**, 3385 (1992).
[13] R. Kretschmer, and K. Binder, Z. Phys. B: Condens. Matter **34**, 375 (1979).
[14] A.M. Ferrenberg, D.P. Landau, and K. Binder, J. Stat. Phys. **63**, 867 (1991).
[15] M.S.S. Challa, and D.P. Landau, Phys. Rev. B **34**, 1841 (1986); A. Billoire, R. Lacaze, A. Morel, S. Gupta, A. Irbäck, and B. Petersson, *ibid.* **42**, 6743 (1990).
[16] R.J. Baxter, J. Phys. C **6**, L445 (1973).
[17] M.H. Cohen and F. Keffer, Phys. Rev. **99**, 1128 (1955).